

Invasiveness of plant pathogens depends on the spatial scale of host distribution

Article

Accepted Version

Mikaberidze, A., Mundt, C. C. and Bonhoeffer, S. (2016)
Invasiveness of plant pathogens depends on the spatial scale
of host distribution. *Ecological Applications*, 26 (4). pp. 1238-
1248. ISSN 0051-0761 doi: <https://doi.org/10.1890/15-0807>
Available at <https://centaur.reading.ac.uk/86101/>

It is advisable to refer to the publisher's version if you intend to cite from the work. See [Guidance on citing](#).

To link to this article DOI: <http://dx.doi.org/10.1890/15-0807>

Publisher: Ecological Society of America

All outputs in CentAUR are protected by Intellectual Property Rights law, including copyright law. Copyright and IPR is retained by the creators or other copyright holders. Terms and conditions for use of this material are defined in the [End User Agreement](#).

www.reading.ac.uk/centaur

CentAUR

Central Archive at the University of Reading

Reading's research outputs online

Invasiveness of plant pathogens depends on the spatial scale of host distribution

Alexey Mikaberidze^{*,1},
Christopher C. Mundt²,
Sebastian Bonhoeffer¹

*alexey.mikaberidze@env.ethz.ch, Institute of Integrative Biology, ETH Zurich, CHN H 75.1,
Universitaetstrasse 16, 8092, Zurich, phone: +41 44 632 26 02

¹Institute of Integrative Biology, ETH Zurich

²Department of Botany and Plant Pathology, Oregon State University

Abstract

Plant diseases often cause serious yield losses in agriculture. A pathogen's invasiveness can be quantified by the basic reproductive number, R_0 . Since pathogen transmission between host plants depends on the spatial separation between them, R_0 is strongly influenced by the spatial scale of the host distribution.

We present a proof of principle of a novel approach to estimate the basic reproductive number, R_0 , of plant pathogens as a function of the size of a field planted with crops and its aspect ratio. This general approach is based on a spatially-explicit population dynamical model. The basic reproductive number was found to increase with the field size at small field sizes and to saturate to a constant value at large field sizes. It reaches a maximum in square fields and decreases as the field becomes elongated. This pattern appears to be quite general: it holds for dispersal kernels that decrease exponentially or faster as well as for fat-tailed dispersal kernels that decrease slower than exponential (i.e. power-law kernels).

We used this approach to estimate R_0 in wheat stripe rust (an important disease caused by *Puccinia striiformis*), where we inferred both the transmission rates and the dispersal kernels from the measurements of disease gradients. For the two largest datasets, we estimated R_0 of *P. striiformis* in the limit of large fields to be of the order of 30. We found that the spatial extent over which R_0 changes strongly is quite fine-scaled (about 30 m of the linear extension of the field). Our results indicate that in order to optimize the spatial scale of deployment of fungicides or host resistances, the adjustments should be made at a fine spatial scale. We also demonstrated how the knowledge of the spatial dependence of R_0 can improve recommendations with regard to fungicide treatment.

Keywords: basic reproductive number, disease control, disease gradient, dispersal, epidemiology, host-pathogen interaction, mathematical model, plant disease, population dynamics, spatial scales

1 Introduction

When plant pathogens succeed in infecting their hosts, they colonize the host tissue and deprive hosts of resources and energy. This often leads to serious yield losses in agriculture (Strange and Scott, 2005). Disease-resistant crop varieties and chemicals (fungicides or antibiotics) are widely used to control infectious diseases of plants. But both of these control measures are highly vulnerable to pathogen adaptation: pathogens evolve to overcome host resistances and to become insensitive to fungicides (McDonald and Linde, 2002). In order to devise effective and durable strategies of disease control (Mundt, 2014), a thorough understanding of basic epidemiological properties of plant pathogens with the help of appropriate mathematical models is necessary. The spread of infectious diseases depends on the contact structure, a network in which each host is a node and has a number of weighted, directional links to other hosts. The strength of each link represents the probability of transmission from one host to another. In infectious diseases of humans and animals contact structures are determined by networks of social contacts. Plant pathogens spread over global scales of countries and continents by natural means and through networks of trade and exchange (Brown and Hovmoller, 2002; Shaw and Pautasso, 2014). However, at a local scale of a single field of crop plants or several adjacent fields, plant pathogens spread primarily through passive dispersal of infectious propagules through air, water or soil between immobile plants. Insect pests may disperse both actively and passively between hosts plants (Mazzi and Dorn, 2012). In both of these cases, the probability of transmission between hosts depends on the geographical distance between them. Hence, the contact structure is determined by the spatial scales of pathogen dispersal and the spatial scales of the host population. Full information on the contact structure is difficult to obtain and to analyze. Several global measures are used to characterize networks of contacts, such as the average degree, i. e. the average

49 number of links per host. Yet, a better measure that characterizes the disease spread is its basic
50 reproductive number, R_0 , defined intuitively as “the average number of secondary cases of
51 infection generated by one primary case in a susceptible host population” (Anderson and May,
52 1986). Mathematically, it is given by the dominant eigenvalue of the next generation operator
53 (Heesterbeek, 2002). Hence, the basic reproductive number is a quantity with a clear biological
54 meaning that characterizes reproductive fitness of the pathogen. In deterministic models, it
55 determines the invasion threshold: if $R_0 > 1$ the disease will spread in the population, otherwise at
56 $R_0 < 1$ the pathogen will eventually die out. Therefore, R_0 can be used to estimate the critical
57 proportion of the host population that needs to be immunized (i. e. vaccinated) in order to eradicate
58 the disease (Anderson and May., 1991). Also, R_0 often allows one to estimate the final
59 (equilibrium) disease level.

60 Much attention has been devoted to estimation of R_0 for infectious diseases of humans and animals
61 (Anderson and May., 1991; Fraser et al., 2009; Hampson et al., 2009). Several studies discuss R_0 in
62 the context of infectious diseases of plants (Gubbins et al., 2000; Park et al., 2001; Parnell et al.,
63 2005; van den Bosch et al., 2008; van den Berg et al., 2011), and in (Montarry et al., 2010) was
64 estimated for potato late blight. But only one study provided estimates for wheat stripe rust
65 (Segarra et al., 2001) based on measurements of the apparent infection rate r (the rate of growth of
66 the disease proportion over time, assuming logistic growth (Vanderplank, 1963)). Another approach
67 is to estimate R_0 by fitting the solution of a population dynamics model of disease spread to an
68 empirical disease progress curve (i. e. the plot of the proportion of disease over time). However, this
69 appears to be difficult, because we expect R_0 to depend on the spatial scales of the host population.
70 In an agricultural setting, crop plants are usually arranged in nearly rectangular fields. Each field is
71 characterized by its area S and aspect ratio α . Hence, R_0 should depend on S and α , provided that
72 the planting density is fixed. Given the wide variation in field sizes and shapes across individual

73 fields and growing regions, countries and continents, a useful estimate for R_0 should also capture
74 the dependence on the field size and shape. But measuring disease progress curves in many fields
75 with different sizes and shapes requires enormous efforts and resources.

76 In this study we propose a novel way to estimate the basic reproductive number R_0 as a function of
77 field size and shape. This approach uses a spatially explicit population dynamics model formulated
78 as a system of integro-differential equations. In this approach, estimation of R_0 requires knowledge
79 of a dispersal kernel, a function that describes dispersal properties of the pathogen. In general,
80 estimation of dispersal kernels is a highly non-trivial problem, as often only limited
81 spatially-resolved disease data is available. Here, we estimate dispersal kernels using disease
82 gradient measurements in which the amount of disease is characterized as a function of the distance
83 from a localized source of initial inoculum. These measurements are only possible for some plant
84 disease systems, while in other cases only limited disease data can be obtained. In these cases,
85 more elaborate statistical methods are necessary to estimate dispersal kernels (Filipe et al., 2012;
86 Gibson et al., 2006).

87 To provide a proof of principle for this method of estimating R_0 , we applied it to wheat stripe rust
88 (an important pathogen of wheat caused by *Puccinia striiformis* (Wellings, 2011)), since disease
89 gradients for this pathogen were thoroughly measured over large distances (Sackett and Mundt,
90 2005a; Cowger et al., 2005). Using these data, we estimated R_0 as a function of the field size and
91 shape. From this dependence we determined the ranges of field sizes and shapes over which R_0
92 exhibits a considerable change. The advantage of this approach is that, by measuring the disease
93 gradient over a large enough distance in a single experiment, one captures the information on the
94 dependence of R_0 on the field size and aspect ratio. In this way, more useful information can be
95 extracted from disease gradient data than thought previously.

2 Methods

We assume that the hosts are continuously distributed across the rectangular field with the dimensions d_x and d_y . The field area is $S = d_x d_y$ and its aspect ratio is $\alpha = d_x/d_y$, so that α close to zero refers to long, narrow fields, while $\alpha = 1$ represents a square field. We trace the densities of healthy hosts $H(x, y, t)$, infected hosts $I(x, y, t)$ and removed hosts $R(x, y, t)$ in space and time using the system of integro-differential equations

$$\frac{\partial H(x, y, t)}{\partial t} = r_H H(x, y, t) [1 - H(x, y, t)/K] - \beta \lambda(x, y) H(x, y, t), \quad (1)$$

$$\frac{\partial I(x, y, t)}{\partial t} = \beta \lambda(x, y) H(x, y, t) - \mu I(x, y, t). \quad (2)$$

$$\frac{\partial R(x, y, t)}{\partial t} = \mu I(x, y, t). \quad (3)$$

Here, the force of infection $\lambda(x, y)$ at a location x, y is determined by integrating over all possible sources of infection:

$$\lambda = \int_0^{d_x} du \int_0^{d_y} dv \kappa(x, y, u, v) I(u, v, t). \quad (4)$$

In obtaining Eqs. (1)-(3) we assumed that the characteristic time scale of spore dispersal is much shorter than the characteristic time scales associated with other stages of the pathogen life cycle and, hence, the density of spores is proportional to the density of the infectious host tissue (see Appendix A.4 in Supporting Information for more details). We also neglected the latent compartment consisting of hosts that are infected but not yet infectious, in spite of the fact that average duration of latent infection was estimated to be around 10 days in wheat stripe rust (van den Bosch et al., 1988; Sache and Vallavieille-Pope, 1993). This simplification is justified because here we focus on determining R_0 , the basic reproductive number, at the starting phase of

118 the epidemic. This phase corresponds to the beginning of the growing season of wheat, when the
 119 senescence of leaves (natural death of hosts) is negligibly small. Under these conditions, latently
 120 infected hosts are likely to survive and be transformed into infectious hosts. Hence, the basic
 121 reproductive is not affected by latency. At the same time, latency of stripe rust played an important
 122 role in distinguishing the primary disease gradients from subsequent pathogen generations when
 123 collecting the data (Sackett and Mundt, 2005a) that we analyze here.

124 The quantities $H(x, y, t)$, $I(x, y, t)$ and $R(x, y, t)$ represent the areas of the corresponding host
 125 tissue per unit land area. The host tissue could be leaves, stems or grain, depending on the specific
 126 host-pathogen interaction. Healthy hosts $H(x, y, t)$ grow logistically with the rate r_H and the
 127 “carrying capacity” K , which may imply limited space or nutrients. We consider a single growing
 128 season and neglect leaf senescence. Furthermore, healthy hosts may be infected by the pathogen
 129 and transformed into infected hosts with the rate $\beta\lambda(x, y)$. The transmission rate β is a compound
 130 parameter given by the product of the sporulation rate of the infected tissue and the probability that
 131 a spore causes new infection. Infected host tissue loses its infectivity at a rate μ , where μ^{-1} is the
 132 average infectious period. In this way, infected hosts $I(x, y, t)$ are continuously transformed into
 133 removed hosts $R(x, y, t)$. Here, $R(x, y, t)$ quantifies the amount of host tissue that was previously
 134 infected, but subsequently lost its ability to produce infectious spores and cannot be re-infected. To
 135 complete the initial-value problem, the initial conditions for the system of Eqs. (1)-(3) can be
 136 defined as, $H(x, y, t = 0) = H_0(x, y)$, $I(x, y, t = 0) = I_0(x, y)$, $R(x, y, t = 0) = R_0(x, y)$. Most
 137 of the results of this study were obtained from the solution of the eigenvalue problem [Eq. (6)
 138 below] that does not require initial conditions. The results in Sec. 3.3 were obtained using an
 139 approximate spatially uniform model. Accordingly, in Sec. 3.3 we used spatially uniform initial
 140 conditions: $H(x, y, t = 0) = H_0$, $I(x, y, t = 0) = I_0$, $R(x, y, t = 0) = 0$. The border condition
 141 requires $H(x, y, t) = 0$ for all x, y that lie outside the field. An approximate version of the model

142 Eqs. (1)-(3), in which the host densities were assumed to be homogeneous in space, was used in
 143 several previous studies of plant disease epidemics (Hall et al., 2007; van den Bosch and Gilligan,
 144 2008; Mikaberidze et al., 2014b).

145 The integral in Eq. (4) is weighted using $\kappa(x, y, u, v)$, the dispersal kernel (or contact distribution
 146 (Mollison, 1977)) that characterizes dispersal properties of the pathogen. The dispersal properties
 147 as well as the environmental conditions are assumed to be the same along the field. Moreover,
 148 dispersal is assumed to be isotropic, meaning that a spore has the same probability to move in any
 149 direction along the two-dimensional field. The latter assumption can be problematic when strong
 150 winds prevail in a certain direction and may be the cause of discrepancy with the empirical findings.
 151 In this case, the dispersal kernel is only determined by the distance

$$152 \quad r = \sqrt{(x - u)^2 + (y - v)^2} \quad (5)$$

153 between the source and the target of infection, i. e. $\kappa(x, y, u, v) = \kappa(r)$. For aerially dispersed plant
 154 diseases, $\kappa(r)$ is defined as a probability density function for an infectious spore to land at a
 155 distance r from its source (Nathan et al., 2012).

156 In order to determine the basic reproductive number, R_0 , we perform the linear stability analysis of
 157 the disease-free equilibrium $H(x, y, t) = K, I(x, y, t) = 0, R(x, y, t) = 0$ of the system
 158 Eqs. (1)-(2). Essentially, we examine whether small deviations from the disease-free equilibrium
 159 grow or die out. This leads to the eigenvalue problem for the Fredholm equation of the second kind
 160 (see Appendix A.1 for the derivation)

$$161 \quad R_{0\infty} \int_0^{d_x} du \int_0^{d_y} dv \kappa(r)w(u, v) = \sigma w(x, y), \quad (6)$$

162 where $R_{0\infty} = \beta K/\mu$ is the basic reproductive number in the limit of a very large field. Definition

163 of $R_{0\infty}$ here, requires that $\mu > 0$. This holds for wheat stripe rust, where the infectious period was
 164 estimated to be $\mu^{-1} \approx 30$ days (Sache and Vallavieille-Pope, 1993). Also, this infectious period is
 165 shorter than the duration of the growing season of wheat. By solving the eigenvalue problem
 166 Eq. (6), we can find the eigenvalues σ_i and eigenfunctions $w_i(x, y)$ that satisfy the Eq. (6). The
 167 dominant eigenvalue σ_d determines the basic reproductive number, i. e. $R_0 = \sigma_d$.
 168 An approximate expression for the basic reproductive number for the model Eqs. (1)-(2) can be
 169 found by applying its intuitive definition (Anderson and May, 1986) and averaging over the spatial
 170 coordinates. This leads to the expression:

$$171 \quad R_{0c}(x_0, y_0) = \frac{\beta K}{\mu} \int_0^{d_x} dx \int_0^{d_y} dy \kappa(x, y, x_0, y_0), \quad (7)$$

172 where we set $H(x, y, t = 0) = K$, $I(x, y, t = 0) = I_{\text{tot}0} \delta(x - x_0) \delta(y - y_0)$, $R(x, y, t = 0) = 0$.
 173 Here, the approximate basic reproductive number depends on the position x_0, y_0 of the initial
 174 inoculum, in contrast to the exact basic reproductive number determined from Eq. (6), which is
 175 independent on the position of the initial inoculum. The approximate basic reproductive number in
 176 Eq. (7) does not yield the invasion threshold at $R_{0c}(x_0, y_0) = 1$ (Diekmann et al., 1990). However it
 177 may serve as a useful approximate expression, since the calculation according to Eq. (7) is often
 178 much simpler than the solution of the eigenvalue problem Eq. (A.3). We found (Appendix A.2) that
 179 the approximate expression for the basic reproductive number Eq. (7) generally underestimates the
 180 actual R_0 , because it neglects the contribution of the subsequent generations of infection. But it
 181 holds well in the two limiting cases: at small field sizes (i. e. when $d \ll a$) and at large field sizes
 182 (i. e. when $d \gg a$).

183 R_0 is computed by numerically solving the eigenvalue problem in Eq. (6) for different values of the
 184 field dimensions d_x and d_y that characterize the field size and shape. Before performing this

185 calculation, we estimated the dispersal kernel $\kappa(r)$ and the compound parameter $R_{0\infty}$ from
 186 experimental data (Sackett and Mundt, 2005a; Cowger et al., 2005) [see Appendix A.3 for the
 187 details of the estimation procedure].

188 In these experiments, winter wheat cultivar Jacmar was planted in three replicate plots measuring
 189 6.1 m wide by 128 to 171 m long, oriented parallel to the dominant wind direction (see Fig. 1 in
 190 (Sackett and Mundt, 2005a)). Small areas of experimental plots (foci) were artificially inoculated
 191 by pathogen spores (0th generation). These spores give rise to lesions in the focus (first generation)
 192 that further produce spores, which are dispersed through the air. This results in infection outside of
 193 the focus, producing the second generation of pathogen lesions. The corresponding disease severity
 194 (the proportion of the leaf area infected) is measured as a function of the distance r from the focus.
 195 We are confident that the observed disease patterns result primarily from the artificial inoculum in
 196 the focus, rather than natural infection, because stripe rust levels were overall very light in Oregon
 197 in 2002 (Long, 2003). Further, disease levels declined consistently with distance and often reached
 198 zero at the farther distances from the inoculum source, which would not be expected if there was
 199 significant inoculum from outside of the plots.

200 When considering fungicide treatment (Sec. 3.3), we take into account the effect of the fungicide on
 201 the transmission rate of the pathogen using the expression

$$202 \quad \beta(D) = \beta_0 [1 - \varepsilon(D)], \quad (8)$$

203 where the fungicide efficacy, $\varepsilon(D)$, is given by the Hill's function

$$204 \quad \varepsilon(D) = \varepsilon_m \frac{D}{D + D_{50}} \quad (9)$$

205 and describes the proportion by which the transmission rate is reduced by the fungicide. In Eq. (9),

206 D is the fungicide dose, ε_m is the maximum fungicide effect at high doses, and D_{50} is the dose at
207 which half of the maximum effect is achieved.

208 **3 Results**

209 **3.1 Dependence of the basic reproductive number on the field size**

210 The basic reproductive number, R_0 , is shown in Fig. 1 as a function of the linear extension d of a
211 square field for three different dispersal kernels (Gaussian, exponential and modified power-law).

212 These three functional forms are often used to describe dispersal gradients in plant diseases (Fitt
213 et al., 1987; Frantzen and Bosch, 2000; Sackett and Mundt, 2005a), but also in other taxonomic
214 groups, for example, in pollen, seeds, seedlings, beetles, moths and butterflies (Nathan et al., 2012).

215 These three functions represent the three classes of dispersal kernels: “thin-tailed” (Gaussian) that
216 decrease faster than exponential, exponential, and “fat-tailed” that decrease slower than exponential
217 (power-law). “Thin-tailed” and exponential kernels give rise to travelling epidemic waves with a
218 constant velocity, while the “fat-tailed” kernels result in accelerating epidemic waves (Mollison,
219 1977; Medlock and Kot, 2003; Cowger et al., 2005; Sackett and Mundt, 2005b).

220 For all the three types of dispersal kernels that we considered, the basic reproductive number first
221 increases as a function of the field size d and then, eventually, saturates to a constant value (Fig. 1).
222 Thus, we find that the qualitative dependence of R_0 , a more basic epidemiological parameter than
223 the epidemic velocity, on the field size is quite robust with respect to the functional form of the
224 dispersal kernel. In particular, it is not affected much by the nature of the tails of the dispersal
225 kernel. Moreover, we expect this behaviour to hold for any dispersal kernel, as long as it a
226 monotonically decreasing function of the distance r .

227 The initial growth of R_0 versus d follows a quadratic function (see Eq. (A.10)). It occurs because in

228 this range, the field size is much smaller than the dispersal radius a (a characteristic length scale of
229 pathogen dispersal), i. e. $d \ll a$. Therefore, by making the field larger, more spores will land within
230 the field and lead to new infections. In other words, in this range the field size is the limiting factor
231 for the pathogen fitness. On the contrary, when the field size is much larger than the dispersal
232 radius, i. e. $d \gg a$, the basic reproductive number becomes independent of d . Here, pathogen does
233 not become fitter on a larger field, because its fitness is now limited by the range of dispersal and
234 not by the size of the field.

235 While the three curves in Fig. 1 exhibit a universal qualitative behaviour, they differ in the rate at
236 which the saturation occurs at large field sizes. The Gaussian dispersal kernel decreases faster with
237 the distance r than the exponential dispersal kernel. As a result, R_0 grows and saturates as a
238 function of the field size d faster for the Gaussian than for the exponential. The result for the
239 power-law dispersal kernel is difficult to compare with the results for other kernels, since the power
240 law lacks a meaningful characteristic length scale. Asymptotically, at large field sizes R_0
241 approaches the constant value slower in the case of the power-law dispersal kernel than for the
242 other two kernels. However, at small field sizes, R_0 as a function of d may grow faster or slower for
243 the power-law kernel as compared to the other two kernels, depending on the values of the
244 parameters r_0 and b . In Fig. 1, we present an example when the R_0 for the power law first grows
245 faster than that for the Gaussian or exponential dispersal kernels, but subsequently its growth slows
246 down and becomes slower than for the Gaussian and exponential (as expected from the asymptotic
247 behavior of the corresponding dispersal kernels).

248 **3.2 Case study: dependence of the basic reproductive number on the** 249 **field size and shape for wheat stripe rust**

250 We infer the dependence of the basic reproductive number, R_0 , on the field size and shape from the
 251 detailed measurements of primary disease gradients of wheat stripe rust (Sackett and Mundt,
 252 2005a; Cowger et al., 2005). The outcome of this measurement is shown in Fig. 2 for the two
 253 largest datasets (Hermiston 2002 and Madras 2002, downwind) obtained in this experiment. These
 254 two datasets were chosen because they contained measurements over large enough distances that
 255 allowed us to obtain sound fits. Disease severity strongly depends on the distance r : the value is
 256 largest closer to the focus and decreases monotonically with r . The data can be fitted well by the
 257 modified power-law function (solid curve in Fig. 2)

$$258 \quad \kappa_{\text{PL2}}(r) = \kappa_0 (r_0^2 + r^2)^{-b/2}. \quad (10)$$

259 In contrast, exponential and Gaussian functions provide poor fits (dashed and dotted curves in
 260 Fig. 2). (For more details on fitting see Appendix A.3.1 and Fig. 6 in the Electronic Supplementary
 261 Materials).

262 Disease gradients, measured in this way, contain information on the three key processes in the
 263 pathogen life-cycle: spore production, aerial movement of spores, and infection of healthy host
 264 tissue. We assume that the rate of spore production and the probability to infect healthy host tissue,
 265 once the spore has landed on it, are homogeneous across the field, i. e. do not depend on the
 266 distance r between the source and the target of infection [Eq. (5)]. Hence, the compound parameter
 267 $R_{0\infty} = \beta K / \mu$ that characterizes these processes does not depend on the distance r . Therefore, the
 268 aerial movement of spores is the only process that depends on the distance r . Further, we assume
 269 that there is a large enough number of spores produced and the probability of infection is large

270 enough such that the recorded disease severity is proportional to the spore concentration in the air.
 271 Under these assumptions, our estimate for the dispersal kernel $\kappa(r)$ is the modified power-law
 272 function [Eq. (10)] fitted to the disease gradient data and normalized as a probability density
 273 function (i. e. such that its integral over the whole two-dimensional space equals to unity
 274 [Appendix A.3.2]). We also estimated the parameter $R_{0\infty}$ from the disease gradient data (see
 275 Appendix A.3.3) and obtained the value $R_{0\infty} = 35 \pm 3$ for the Hermiston 2002 downwind dataset;
 276 and the value $R_{0\infty} = 23 \pm 4$ for the Madras 2002 downwind dataset.
 277 Using our estimates for the dispersal kernel, $\kappa(r)$, and the parameter $R_{0\infty}$ we solved the eigenvalue
 278 problem Eq. (6) numerically for different field sizes and shapes. In this way, we obtained the
 279 dependence of the basic reproductive number R_0 on the field size (Fig. 3) and its aspect ratio
 280 (Fig. 4). In Fig. 3, R_0 first grows steeply versus the linear extension of a square field and saturates
 281 towards the asymptotic value $R_{0\infty}$ for large fields. The basic reproductive number is about two
 282 times larger for the parameter values corresponding to Hermiston 2002 dataset, than for the case of
 283 Madras 2002 dataset. This difference stems from the difference in the asymptotic values $R_{0\infty}$ and
 284 also from different shapes of the disease gradients (cf. panel (a) and (b) in Fig. 2).
 285 The asymptotic value, $R_{0\infty}$, (indicated by the horizontal dashed line in Fig. 3), is approached faster
 286 in the case of Hermiston 2002 dataset (solid curve in Fig. 3), than for Madras 2002 dataset (dashed
 287 curve in Fig. 3). The reason for this is a different exponent of the power-law function that best fits
 288 the corresponding disease gradients ($b = 3.04$ for Hermiston 2002, Eq. (A.15), and $b = 2.23$,
 289 Eq. (A.16)). The disease gradient in Madras 2002 decreases slower due a lower exponent.
 290 In Fig. 4, R_0 exhibits a saturating growth as the field aspect ratio α is increased from 0.01 to 1.
 291 Hence, the square fields, with $\alpha = 1$, are most conducive for the disease growth. The basic
 292 reproductive number grows faster and saturates at larger values of α in smaller fields (cf. dotted,
 293 dashed, dash-dotted and solid curves in Fig. 4).

294 A number of empirical studies have reported that, in agreement with our results, smaller plots
295 resulted in lower disease levels in wheat stripe rust (Mundt et al., 1996), wheat brown rust
296 (*Puccinia recondita* f. sp. *tritici*) (Bowen et al., 1984), potato late blight (Paysour and Fry, 1983)
297 and *Valdensia heterodoxa* on *Vaccinium myrtillus* (Strengbom et al., 2006). However, in a more
298 recent study in wheat stripe rust (Sackett and Mundt, 2009) that used considerably larger plot sizes,
299 the plot size did not affect the epidemic velocity. Our estimation framework predicts moderate
300 differences in the values of R_0 between larger square plots and smaller elongated plots used in
301 experiments (Sackett and Mundt, 2009) (cf. the white and gray circles in both panels of Fig. 4).
302 This is expected to result in higher epidemic velocities in larger plots compared to smaller plots,
303 according to theoretical arguments (Keeling and Rohani, 2008). We suggest two possible
304 explanations for this discrepancy. First, strong wind with a prevailing direction along the axis of the
305 elongated plot was observed in the experimental setting (Sackett and Mundt, 2009), but in our
306 model isotropic dispersal was assumed. The differences in R_0 between smaller elongated plot and a
307 larger square plot that we predict using the model are possibly masked by the wind. This is because
308 the wind may increase the pathogen's R_0 in the smaller elongated plot by preventing the spores to
309 land outside the plot. Second, a moderate difference of 20-30 % that we predict for epidemic
310 velocities may be difficult to detect given the level of experimental uncertainties.

311 **3.3 Effect of the plot size on the fungicide dose-response**

312 Control of stripe rust greatly relies on fungicides. Field experiments, in which disease severity is
313 measured as a function of the fungicide dose, inform strategies of fungicide treatment. These
314 experiments are typically performed on rather small fields, in the range of 20-60 m². The outcomes
315 are used to choose appropriate fungicide doses (Paveley et al., 1998).

316 How do the sizes of experimental plots affect the outcomes of dose-response measurements? What

317 implications does it have for disease control? Figure 5 illustrates the effect of the plot size on the
318 fungicide dose-response as predicted by the model. Severity of stripe rust [panel (a)] and the
319 pathogen's basic reproductive number, R_0 , [panel (b)] are shown versus the fungicide dose for two
320 field sizes: 60 m^2 (solid) and 90 m^2 (dashed). We fitted the solid curve in Fig. 5 (a) to the
321 dose-response data (Bounds et al., 2012) (filled triangles), while the other three curves in Fig. 5(a,b)
322 were devised from it using theoretical considerations. In particular, we chose to use a non-spatial
323 approximation to the full solution of the system of Eq. (1)-(3), which assumes homogeneous
324 mixing and more specifically assumes that the disease severity changes over time according to a
325 logistic function [Eq. (A.49) in Appendix A.5]. This choice is justified, because there is no
326 availability of empirical data on spatial dynamics within individual field-plots in fungicide
327 dose-response experiments. Nevertheless, the effect of the spatial extension is incorporated through
328 the dependence of the basic reproductive number, R_0 , on the field size that was determined above.
329 We also assumed that the field size and the fungicide affect the basic reproductive number
330 independently, hence their effects enter as multiplicative factors. (Please refer to Appendix A.5 for
331 details).

332 Disease severity strongly depends on both the fungicide dose and the field size (cf. solid and
333 dashed curves in Fig. 5(a)). R_0 also depends on both the fungicide dose and the field size (cf. solid
334 and dashed curves in Fig. 5(b)), but the changes in R_0 are less pronounced than changes in disease
335 severity. Hence, in this parameter regime of large R_0 -values, moderate changes in R_0 may lead to
336 considerable changes in disease severity.

337 What do these insights mean for disease control? First, achieving good disease control in a
338 relatively small plot ($\lesssim 100 \text{ m}^2$) does not guarantee good control in larger fields. For example, in
339 the 60 m^2 plot, disease severity of $< 5 \%$ was reached at a fungicide dose $D = 0.25$ [solid curve in
340 Fig. 5(a)]. But in a larger field of 90 m^2 this dose was able to reduce the severity only down to about

341 30 % [dashed curve in Fig. 5(a)]. Therefore, typical dose-response measurements that are
342 performed in the range of field sizes of 30-60 m² may strongly underestimate the disease severity in
343 larger fields used by growers. As a result, recommendations with regard to fungicide dosage and
344 other control options based on dose-response measurements in small fields may be unreliable.
345 However, a considerable increase in sizes of experimental plots seems impractical, because it
346 would greatly increase the costs. Moreover, even when using larger plots, one would still not be
347 certain that the plot is large enough to reach saturation. Here, we propose a more economical
348 alternative. Using the dependence of the basic reproductive number, R_0 , on the plot size in the
349 absence of fungicides, this approach allows to extrapolate a dose-response curve, measured for a
350 particular plot size, to other plot sizes. Figure 5 illustrates possible outcomes. Based on the
351 empirical dose-response curve for the 60 m² plot and the dependence of R_0 on the plot size for
352 stripe rust that we determined above in Sec. 3.1 (Fig. 3), we found the dependence of R_0 on the
353 fungicide dose for different field sizes [Fig. 5(b)]. After that, we computed dose-response curves at
354 different field sizes: an example for a somewhat larger field of 90 m² is shown as a dashed curve in
355 Fig. 5(a). Thus, the scenario shown in Fig. 5 illustrates how the knowledge of the basic reproductive
356 number can inform strategy of fungicide application. These results should not be considered as
357 quantitatively exact, because we combined the fungicide dose-response data and disease gradient
358 data from different locations. But we believe they illustrate a useful principle and reflect correctly
359 important qualitative trends.

360 4 Discussion

361 We found that the basic reproductive number, R_0 , of crop pathogens depends on the size and
362 geometry of the field planted with host plants using a single-field, single-season epidemic model.

363 R_0 increases with the field size at small field sizes and saturates to a constant values at large field
364 sizes. The value of R_0 reaches its maximum in square fields and decreases as the field becomes
365 elongated, while retaining the same area. This is because for smaller and more elongated fields, a
366 larger number of pathogen spores will land outside the field and not reach host plants. This pattern
367 appears to be quite general: it holds for dispersal kernels that decrease exponentially or faster (i. e.
368 Gaussian kernels) as well as for “fat-tailed” dispersal kernels that decrease slower than exponential
369 ones (i. e. power-law kernels). We expect the same qualitative behavior for any dispersal kernel,
370 provided that it is a monotonically decreasing function of the distance r between the source and the
371 target of infection.

372 As expected, this qualitative picture also holds for the dispersal kernels estimated in wheat stripe
373 rust. The asymptotic values of the basic reproductive number at large field sizes ($R_{0\infty} = 35 \pm 3$ for
374 Hermiston 2002, $R_{0\infty} = 23 \pm 4$ for Madras 2002 dataset) are noticeably smaller than the estimate
375 of around 60 that was obtained (Segarra et al., 2001) from the measurements of the apparent rate of
376 infection r (van den Bosch et al., 1988). This difference may result from differences in wheat
377 cultivars, pathogen strains and environmental conditions in these field experiments.

378 We assumed that the pathogen dispersal is isotropic with the dispersal kernel estimated from the
379 downwind disease gradient. This is a major simplification that will affect the dependence of R_0 on
380 field size and field geometry. Anisotropy of the dispersal kernels was detected in *P. striiformis*
381 Soubeyrand et al. (2007) and *Mycosphaerella fijiensis* Rieux et al. (2014), an important pathogen of
382 banana trees. However, we expect that this assumption does not influence much our estimates of
383 $R_{0\infty}$. This is because $R_{0\infty}$ corresponds to the situation when the field is large enough, such that it
384 does not limit pathogen dispersal. Hence, our $R_{0\infty}$ estimates are determined by
385 spatially-independent estimates of the transmission rate that we obtained from downwind disease
386 gradients.

387 The estimates for $R_{0\infty}$ that we obtained for wheat stripe rust are considerably larger than typical
388 estimates for the basic reproductive number for human or animal diseases. For example, the
389 relatively large values of R_0 were estimated for childhood diseases such as measles (14-18) and
390 pertussis (5-18) (Anderson and May., 1991), the estimates for the “swine flu” influenza H1N1 were
391 in the range 1.4-1.6 (Fraser et al., 2009), the estimates for rabies were in the range 1-2 (Hampson
392 et al., 2009). A possible exception is malaria, where the estimates of R_0 between one and more
393 than 3000 were reported (Smith et al., 2007). The R_0 determines the critical proportion p_c of the
394 host population that needs to be immunized in order to eradicate the disease ($p_c = 1 - 1/R_0$)
395 (Anderson and May., 1991). For example, our estimate for the wheat stripe rust of $R_0 \simeq 30$ yields
396 the critical proportion $p_c \simeq 0.97$. This may be one of the factors to explain why it is so difficult to
397 eradicate rusts, while there are cases of dangerous human diseases (for example, small pox) that
398 were eradicated with the help of vaccination programmes (Anderson and May., 1991). This
399 difference in the values of R_0 may result from a different biology of hosts (animals versus plants),
400 or, alternatively, it could be due to different nature of the diseases, i. e. systemic diseases in the case
401 of humans and animals versus local lesion diseases in the case of wheat stripe rust. To determine
402 which of these two explanations is more plausible, one needs to estimate R_0 for systemic disease of
403 plants and local lesion (i. e. skin diseases) of animals. This difference may also be caused by the
404 characteristic features of host populations in agroecosystems, where genetically uniform hosts are
405 planted with high densities in a homogeneous environment. Hence, it would be interesting to
406 compare the R_0 of crop pathogens with the R_0 of plant pathogens in natural ecosystems. To make
407 these comparisons valid, one needs to include seasonal cycles of hosts. In the case of annual crops
408 like wheat, this means the consideration of the “between-season” R_0 , in addition to the
409 “within-season” R_0 discussed in this study.

410 These findings may help manage some plant diseases, if one knows the spatial scales, i. e. field

411 sizes and aspect ratios, over which R_0 changes considerably. We found that the R_0 of wheat stripe
412 rust exhibits a large change at a fine spatial scale: when the linear dimension of a square field
413 increases from zero to about thirty meters (Fig. 3). The most substantial change of R_0 as a function
414 of the field aspect ratio occurs between aspect ratios of 0.01 and 0.2. These results suggest, that
415 decreasing field sizes and elongating fields may not be a practical measure to control wheat stripe
416 rust, because the beneficial effect of lowering the disease levels is in this case unlikely to outweigh
417 the economical costs associated with using smaller and longer fields. But this method could be
418 feasible for controlling other diseases of crops or pests (for example, western corn rootworm that
419 can disperse over longer distances (Carrasco et al., 2010) than wheat stripe rust). We hope that our
420 study will stimulate more detailed empirical characterization of transmission rates and dispersal
421 kernels for different crop pathogens over long enough distances, such that the framework proposed
422 here could be used to infer how the R_0 depends on the spatial scales of the host population.

423 Although similar ideas about possibilities to control plant diseases by adjusting field size and
424 geometry were explored mathematically in (Fleming et al., 1982), their framework based on
425 reaction-diffusion models was not capable of including realistic dispersal kernels. Hence, they
426 could not estimate the spatial scales at which the pathogen fitness changes considerably.

427 The experiments in Hermiston 2002 and Madras 2002 used the same planting density, the same
428 wheat cultivar and the same pathogen race was used for initial inoculation. But the environmental
429 conditions were somewhat different in these two locations. In particular, the inoculation was
430 substantially more successful in Hermiston than in Madras. Hence, we can largely attribute the
431 difference in the disease gradients between these two datasets and the resulting difference in the
432 estimated values of the basic reproductive number to the difference in the environmental
433 conditions. In contrast, in natural epidemics the variation in the outcomes of pathogen dispersal can
434 also result from the genetic variation in pathogen and host population (Tack et al., 2013).

435 Therefore, it would be interesting to explore the effect of simultaneously adjusting the spatial
436 scales and introducing genetic diversity to the host population by using host mixtures or multiline
437 cultivars (Mundt, 2002; Mikaberidze et al., 2014a)

438 From another point of view, our findings could be helpful for choosing the minimum plot sizes and
439 aspect ratios for field experimentation that focuses on transmission properties of plant pathogens.

440 For the experimental plots to be representative of larger fields used by growers in terms of the
441 pathogen's basic reproductive number, the plot size and aspect ratio should be chosen such that they
442 correspond to the start of the saturation of the dependency of R_0 on the field size (Fig. 3) and aspect
443 ratio (Fig. 4). Thus, our results indicate that in the case of wheat stripe rust, the plot area at which
444 saturation starts is about 0.25 ha and the aspect ratio should be at least 0.2 (this corresponds
445 approximately to a 20 m × 110 m elongated plot, or, alternatively, a 50 m × 50 m square plot). In
446 Sec. 3.3 we presented a specific scenario illustrating that the knowledge of the spatial dependence
447 of the basic reproductive number, R_0 , can inform fungicide treatment strategies. Our analysis
448 revealed that in the range of plot sizes typically used to measure the fungicide dose-response curves
449 (20-60 m²), both the disease severity and the basic reproductive number depend strongly on the
450 field size. We proposed a method to extrapolate the dose-response curves measured in small plots
451 to larger plots based on the knowledge of R_0 .

452 Our results could also help to manage fungicide resistance. Several different fungicides may be
453 applied over smaller, elongated patches within a larger field. In a future study, we plan to determine
454 conditions, when this spatial arrangement of fungicide applications gives the sensitive strain a
455 selective advantage over different resistant strains. This may only work for asexually reproducing
456 pathogens, such as wheat stripe rust outside the Himalayan region and surrounding areas. This
457 strategy allows one to keep the overall field size large enough to be economically advantageous, but
458 requires availability of several different fungicides that have little or no cross-resistance. The same

459 reasoning applies also for the case of break-down of disease resistance in host plants. In this case,
460 host cultivars with different disease resistances should be arranged in smaller, elongated patches
461 within a larger field. Favorable arrangements of these patches with different fungicides and host
462 cultivars that would reduce selection for fungicide resistance and minimize break-down of host
463 defences can be investigated using dynamical simulations of the population dynamics model based
464 on Eqs. (1)-(3).

465 So far we discussed disease control on the level of a single field of crops. But in practice, major
466 crops such as wheat are grown in cultivated landscapes that consist of many fields. Consider the
467 situation when the total area of the landscape and its proportion allocated for wheat cultivation are
468 fixed. Under these constraints, what is an optimal arrangement of wheat plots across the landscape
469 in terms of disease control? Our finding that pathogen fitness decreases in smaller and more
470 elongated fields can be used to optimize the spatial structure of cultivated landscapes in the case
471 when every individual field is far enough from other fields such that inter-field pathogen
472 transmission is negligible. This is only possible when the area allocated for wheat cultivation
473 occupies only a moderate fraction of the total landscape area. But if the area allocated for wheat
474 constitutes a large fraction of the total landscape area, making fields smaller will increase their
475 number and bring them closer to each other. Also, elongated fields may lead to better connectivity
476 between fields in terms of pathogen dispersal. These effects will likely increase the pathogen's
477 basic reproductive number over the landscape scale. We expect that the trade-off between the
478 pathogen transmission within individual fields and between different fields will lead to intermediate
479 optimum field sizes and aspect ratios. To quantify these optima, epidemic models need to include
480 both the scale of single fields and the regional landscape scale (Parnell et al., 2006; Papaix et al.,
481 2014). Our study lays a solid foundation for future modeling work in this direction.

Acknowledgements

AM and SB gratefully acknowledge financial support by the ERC advanced grant PBDR 268540 “The population biology of drug resistance: Key principles for a more sustainable use of drugs”. The contributions of CM were supported by NIH grant R01GM96685 through the NSF/NIH Ecology and Evolution of Infectious Disease Program. The authors would like to thank Kathryn Sackett for providing estimates of the apparent infection rate, data on disease gradients from replicate plots and helpful discussions. AM is grateful to Bruce McDonald and Roland Regoes for many valuable discussions. AM and SB are grateful to members of the Theoretical Biology group at the ETH Zurich for fruitful discussions and brainstorming.

References

- Anderson, R. M., and R. M. May. 1986. The invasion, persistence and spread of infectious diseases within animal and plant communities. *Philosophical transactions of the Royal Society of London. Series B, Biological sciences* **314**:533–70.
- Anderson, R. M., and R. M. May. 1991. *Infectious diseases of humans*. Oxford University Press.
- Bounds, P., J. Blake, B. Fraaije, D. Parsons, S. Knight, F. Burnett, J. Spink, and J. McVitte. 2012. Fungicide performance on winter wheat. Home-Grown Cereals Authority, UK, Project Report 488.
- Bowen, K., P. Teng, and A. Roelfs. 1984. Negative Interplot Interference in Field Experiments with Leaf Rust of Wheat. *Phytopathology* **74**:1157–61.
- Brown, J. K. M., and M. S. Hovmoller. 2002. Aerial dispersal of pathogens on the global and continental scales and its impact on plant disease. *Science (New York, N.Y.)* **297**:537–41.

- 503 Carrasco, L., T. Harwood, S. Toepfer, A. MacLeod, N. Levay, J. Kiss, R. Baker, J. Mumford, and
504 J. Knight. 2010. Dispersal kernels of the invasive alien western corn rootworm and the
505 effectiveness of buffer zones in eradication programmes in Europe. *Annals of Applied Biology*
506 **156**:63–77.
- 507 Cowger, C., L. D. Wallace, and C. C. Mundt. 2005. Velocity of spread of wheat stripe rust
508 epidemics. *Phytopathology* **95**:972–82.
- 509 Diekmann, O., J. A. P. Heesterbeek, and J. A. J. Metz. 1990. On the definition and the computation
510 of the basic reproduction ratio R_0 in models for infectious diseases in heterogeneous
511 populations. *Journal of Mathematical Biology* **28**:365–382.
- 512 Filipe, J. A. N., R. C. Cobb, R. K. Meentemeyer, C. A. Lee, Y. S. Valachovic, A. R. Cook, D. M.
513 Rizzo, and C. A. Gilligan. 2012. Landscape epidemiology and control of pathogens with cryptic
514 and long-distance dispersal: sudden oak death in northern Californian forests. *PLoS*
515 *computational biology* **8**:e1002328.
- 516 Fitt, B. D. L., P. H. Gregory, A. D. Todd, H. A. McCartney, and O. C. Macdonald. 1987. Spore
517 Dispersal and Plant Disease Gradients; a Comparison between two Empirical Models. *Journal of*
518 *Phytopathology* **118**:227–242.
- 519 Fleming, R., L. Marsh, and H. Tuckwell. 1982. Effect of field geometry on the spread of crop
520 disease. *Protection Ecology* **4**:81.
- 521 Frantzen, J., and F. V. D. Bosch. 2000. Spread of organisms: can travelling and dispersive waves be
522 distinguished ? *Basic and Applied Ecology* **91**:83–91.
- 523 Fraser, C., C. A. Donnelly, S. Cauchemez, W. P. Hanage, M. D. Van Kerkhove, T. D.
524 Hollingsworth, J. Griffin, R. F. Baggaley, H. E. Jenkins, E. J. Lyons, T. Jombart, W. R. Hinsley,

- 525 N. C. Grassly, F. Balloux, A. C. Ghani, N. M. Ferguson, A. Rambaut, O. G. Pybus,
526 H. Lopez-Gatell, C. M. Alpuche-Aranda, I. B. Chapela, E. P. Zavala, D. M. E. Guevara,
527 F. Checchi, E. Garcia, S. Hugonnet, and C. Roth. 2009. Pandemic potential of a strain of
528 influenza A (H1N1): early findings. *Science (New York, N.Y.)* **324**:1557–61.
- 529 Gibson, G. J., W. Otten, J. A. N. Filipe, A. Cook, G. Marion, and C. A. Gilligan. 2006. Bayesian
530 estimation for percolation models of disease spread in plant populations. *Statistics and*
531 *Computing* **16**:391–402.
- 532 Gubbins, S., C. A. Gilligan, and A. Kleczkowski. 2000. Population dynamics of plant-parasite
533 interactions: thresholds for invasion. *Theoretical Population Biology* **57**:219–33.
- 534 Hall, R. J., S. Gubbins, and C. A. Gilligan. 2007. Evaluating the performance of chemical control
535 in the presence of resistant pathogens. *Bulletin of mathematical biology* **69**:525–37.
- 536 Hampson, K., J. Dushoff, S. Cleaveland, D. T. Haydon, M. Kaare, C. Packer, and A. Dobson. 2009.
537 Transmission dynamics and prospects for the elimination of canine rabies. *PLoS Biology* **7**:e53.
- 538 Heesterbeek, J. 2002. A Brief History of R_0 and a Recipe for its Calculation. *Acta Biotheoretica*
539 **5**:189–204.
- 540 Keeling, M. J., and P. Rohani, 2008. Spatial Models. Chapter 7, page 266 *in* *Modeling Infectious*
541 *Diseases in Humans and Animals*. Princeton University Press, Princeton.
- 542 Long, D., 2003. Estimated small grain losses from rust in 2002
543 http://www.ars.usda.gov/SP2UserFiles/ad_hoc/36400500Smallgrainlossesduetorust/2002loss/02rustloss.pdf.
- 544 Mazzi, D., and S. Dorn. 2012. Movement of insect pests in agricultural landscapes. *Annals of*
545 *Applied Biology* **160**:97–113.

- 546 McDonald, B. A., and C. Linde. 2002. Pathogen population genetics, evolutionary potential, and
547 durable resistance. *Annual Review of Phytopathology* **40**:349–79.
- 548 Medlock, J., and M. Kot. 2003. Spreading disease: integro-differential equations old and new.
549 *Mathematical Biosciences* **184**:201–222.
- 550 Mikaberidze, A., B. McDonald, and S. Bonhoeffer. 2014*a*. Developing smarter host mixtures to
551 control plant disease. *Plant Pathology* in press DOI:0.1111/ppa.12321, e-print arXiv:1402.2788 .
- 552 Mikaberidze, A., B. A. McDonald, and S. Bonhoeffer. 2014*b*. Can high risk fungicides be used in
553 mixtures without selecting for fungicide resistance? *Phytopathology* **104**:324–331.
- 554 Mollison, D. 1977. Spatial Contact Models for Ecological and Epidemic Spread. *Journal of the*
555 *Royal Statistical Society. Series B* **39**:283.
- 556 Montarry, J., F. M. Hamelin, I. Glais, R. Corbi, and D. Andrivon. 2010. Fitness costs associated
557 with unnecessary virulence factors and life history traits: evolutionary insights from the potato
558 late blight pathogen *Phytophthora infestans*. *BMC evolutionary biology* **10**:283.
- 559 Mundt, C. C. 2002. Use of multiline cultivars and cultivar mixtures for disease management.
560 *Annual review of phytopathology* **40**:381–410.
- 561 Mundt, C. C. 2014. Durable resistance: A key to sustainable management of pathogens and pests.
562 *Infection, genetics and evolution: journal of molecular epidemiology and evolutionary genetics*
563 *in infectious diseases* **in press**.
- 564 Mundt, C. C., L. S. Brophy, and S. C. Kolar. 1996. Effect of genotype unit number and spatial
565 arrangement on severity of yellow rust in wheat cultivar mixtures. *Plant Pathology* **45**:215–222.

- 566 Nathan, R., E. Klein, J. J. Robledo-Arnuncio, and E. Revilla, 2012. Dispersal kernels: review.
567 Chapter 15, page 187 in J. Clobert, M. Baguette, T. G. Benton, and J. M. Bullock, editors.
568 Dispersal ecology and evolution. Oxford Univ. Press.
- 569 Papaïx, J., S. Touzeau, H. Monod, and C. Lannou. 2014. Can epidemic control be achieved by
570 altering landscape connectivity in agricultural systems? *Ecological Modelling* **284**:35–47.
- 571 Park, A. W., S. Gubbins, and C. A. Gilligan. 2001. Invasion and persistence of plant parasites in a
572 spatially structured host population. *Oikos* **94**:162–174.
- 573 Parnell, S., C. Gilligan, and F. van den Bosch. 2005. Small-scale fungicide spray heterogeneity and
574 the coexistence of resistant and sensitive pathogen strains. *Phytopathology* **95**:632–9.
- 575 Parnell, S., F. van den Bosch, and C. Gilligan. 2006. Large-scale fungicide spray heterogeneity and
576 the regional spread of resistant pathogen strains. *Phytopathology* **96**:549–55.
- 577 Paveley, N., M. Hims, and D. Stevens. 1998. Appropriate fungicide doses for winter wheat and
578 matching crop management to growth and yield potential. Home-Grown Cereals Authority, UK,
579 Project Report **166**.
- 580 Paysour, R., and W. Fry. 1983. Interplot interference: A model for planning field experiments with
581 aerially disseminated pathogens. *Phytopathology* **73**:1014.
- 582 Rieux, A., S. Soubeyrand, F. Bonnot, E. K. Klein, J. E. Ngando, A. Mehl, V. Ravigne, J. Carlier,
583 and L. De Lapeyre De Bellaire. 2014. Long-distance wind-dispersal of spores in a fungal plant
584 pathogen: Estimation of anisotropic dispersal kernels from an extensive field experiment. *PLoS*
585 *ONE* **9**.
- 586 Sache, I., and C. Vallavieille-Pope. 1993. Comparison of the wheat brown and yellow rusts for

- 587 monocyclic sporulation and infection processes, and their polycyclic consequences. *Journal of*
588 *phytopathology* **138**:55–65.
- 589 Sackett, K. E., and C. C. Mundt. 2005*a*. Primary disease gradients of wheat stripe rust in large field
590 plots. *Phytopathology* **95**:983–91.
- 591 Sackett, K. E., and C. C. Mundt. 2005*b*. The effects of dispersal gradient and pathogen life cycle
592 components on epidemic velocity in computer simulations. *Phytopathology* **95**:992–1000.
- 593 Sackett, K. E., and C. C. Mundt. 2009. Effect of plot geometry on epidemic velocity of wheat
594 yellow rust. *Plant Pathology* **58**:370–377.
- 595 Segarra, J., M. J. Jeger, and F. van den Bosch. 2001. Epidemic dynamics and patterns of plant
596 diseases. *Phytopathology* **91**:1001–10.
- 597 Shaw, M. W., and M. Pautasso. 2014. Networks and Plant Disease Management: Concepts and
598 Applications. *Annual Review of Phytopathology* **52**:in press.
- 599 Smith, D. L., F. E. McKenzie, R. W. Snow, and S. I. Hay. 2007. Revisiting the basic reproductive
600 number for malaria and its implications for malaria control. *PLoS Biology* **5**:e42.
- 601 Soubeyrand, S., J. Enjalbert, A. Sanchez, and I. Sache. 2007. Anisotropy, in density and in
602 distance, of the dispersal of yellow rust of wheat: experiments in large field plots and estimation.
603 *Phytopathology* **97**:1315–24.
- 604 Strange, R. N., and P. R. Scott. 2005. Plant disease: a threat to global food security. *Annual*
605 *Review of Phytopathology* **43**:83–116.
- 606 Strengbom, J., G. Englund, and L. Ericson. 2006. Experimental scale and precipitation modify
607 effects of nitrogen addition on a plant pathogen. *Journal of Ecology* **94**:227–233.

- 608 Tack, A., J. Hakala, T. Petäjä, M. Kulmala, and A. Laine. 2013. Genotype and spatial structure
609 shape pathogen dispersal and disease dynamics at small spatial scales. *Ecology* **95**:703–714.
- 610 van den Berg, F., N. Bacaer, J. S. J. Metz, C. Lannou, and F. van den Bosch. 2011. Periodic host
611 absence can select for higher or lower parasite transmission rates. *Evolutionary Ecology*
612 **25**:121–137.
- 613 van den Bosch, F., H. Frinking, J. Metz, and J. Zadoks. 1988. Focus expansion in plant disease. III:
614 Two experimental examples. *Phytopathology* **78**:919–925.
- 615 van den Bosch, F., and C. A. Gilligan. 2008. Models of fungicide resistance dynamics. *Annu. Rev.*
616 *Phytopathol.* **46**:123–47.
- 617 van den Bosch, F., N. McRoberts, F. van den Berg, and L. Madden. 2008. The Basic Reproduction
618 Number of Plant Pathogens: Matrix Approaches to Complex Dynamics. *Phytopathology*
619 **98**:239–249.
- 620 Vanderplank, J. E. 1963. *Plant Diseases: Epidemics and Control*. Academic Press, New York.
- 621 Wellings, C. R. 2011. Global status of stripe rust: a review of historical and current threats.
622 *Euphytica* **179**:129–141.

623 **Supplemental Material**

624 **Ecological Archives**

625 Appendix A “Mathematical methods and estimation techniques for determination of the basic
626 reproductive number” is available online:

Table 1: Variables and parameters

| | Description | Dimension |
|-------------------|-----------------------------------------------------------------------|--------------------|
| Variables | | |
| $H(x, y, t)$ | Density of healthy host tissue | dl |
| $I(x, y, t)$ | Density of infected host tissue | dl |
| Parameters | | |
| d_x, d_y | Linear dimensions of the field along x and y | m |
| a | Characteristic spatial scale of pathogen dispersal (dispersal radius) | m |
| β | Transmission rate | days ⁻¹ |
| μ^{-1} | Average infectious period | days |
| r_H | Growth rate of healthy host tissue | days ⁻¹ |
| K | “Carrying capacity” of the healthy host tissue | dl |
| $R_{0\infty}$ | Basic reproductive number in the limit of a very large field | dl |
| Functions | | |
| $\kappa(r)$ | Dispersal kernel | m ⁻¹ |
| $R_0(d_x, d_y)$ | Basic reproductive number | dl |
| $\lambda(x, y)$ | The force of infection [Eq. (4)] | |

627 Figure 1. Basic reproductive number R_0 as a function of the field size d for the two-dimensional
 628 field according to the numerical solution of Eq. (6) (solid green) using (i) the Gaussian [Eq. (A.21)]
 629 at $n = 2$, $a = 10$ m], (ii) the exponential [Eq. (A.21) at $n = 1$, $a = 10$ m] and (iii) the power law
 630 dispersal kernel [Eq. (A.19) at $r_0 = 1$ m, $b = 2.1$]. Model parameters: $R_{0\infty} = \beta K/\mu = 2$.

631 Figure 2. Disease severity of wheat stripe rust is plotted as a function of the distance from focus,
 632 according to outcomes of field experiments (Sackett and Mundt, 2005a; Cowger et al., 2005). Two
 633 datasets, Hermiston 2002 downwind (left panel) and Madras 2002 downwind were fitted with the
 634 exponential function [Eq. (A.21) with $n = 1$, dashed curve], the Gaussian function [Eq. (A.21) with
 635 $n = 2$, dotted curve] and the modified power-law function [Eq. (A.19), solid curve].

636 Figure 3. Basic reproductive number R_0 as a function of the field size d of a square field calculated
 637 [by solving numerically the eigenvalue problem Eq. (6)] using the modified power-law dispersal
 638 kernel [Eq. (10)] fitted in Fig. 2 to disease gradient datasets (i) Hermiston 2002 downwind (solid
 639 curve), and (ii) Madras 2002 downwind (dashed curve) obtained in (Sackett and Mundt, 2005a;
 640 Cowger et al., 2005). Horizontal dashed lines show the asymptotic values of the basic reproductive
 641 number at large field sizes, $R_{0\infty}$, for Hermiston 2002 (upper line) and Madras 2002 (lower line)
 642 datasets. Error bars represent 95 % confidence intervals for $R_{0\infty}$ estimates (see Appendix A.3).

643 Figure 4. Basic reproductive number R_0 as a function of the field aspect ratio d_x/d_y (the field area
 644 $S = d_x d_y$ was kept the same). The calculation was performed numerically using the power-law
 645 dispersal kernels fitted to disease gradient data (Fig. 2) from Hermiston 2002 (upper panel) and
 646 Madras 2002 (lower panel) datasets obtained in (Sackett and Mundt, 2005a; Cowger et al., 2005).
 647 Different curves show the R_0 for different field areas: $S = 4$ ha (yellow solid), $S = 1$ ha (blue
 648 dashed), $S = 0.37$ ha (red dash-dotted), $S = 0.04$ ha (orange dotted).

649 Figure 5. Dependence of stripe rust severity (panel (a)) and the basic reproductive number, R_0 ,
650 (panel (b)) on the fungicide dose (epoxiconazole) for two different sizes of square fields:
651 $S = 60 \text{ m}^2$ (blue, solid) and $S = 90 \text{ m}^2$ (red, dashed).

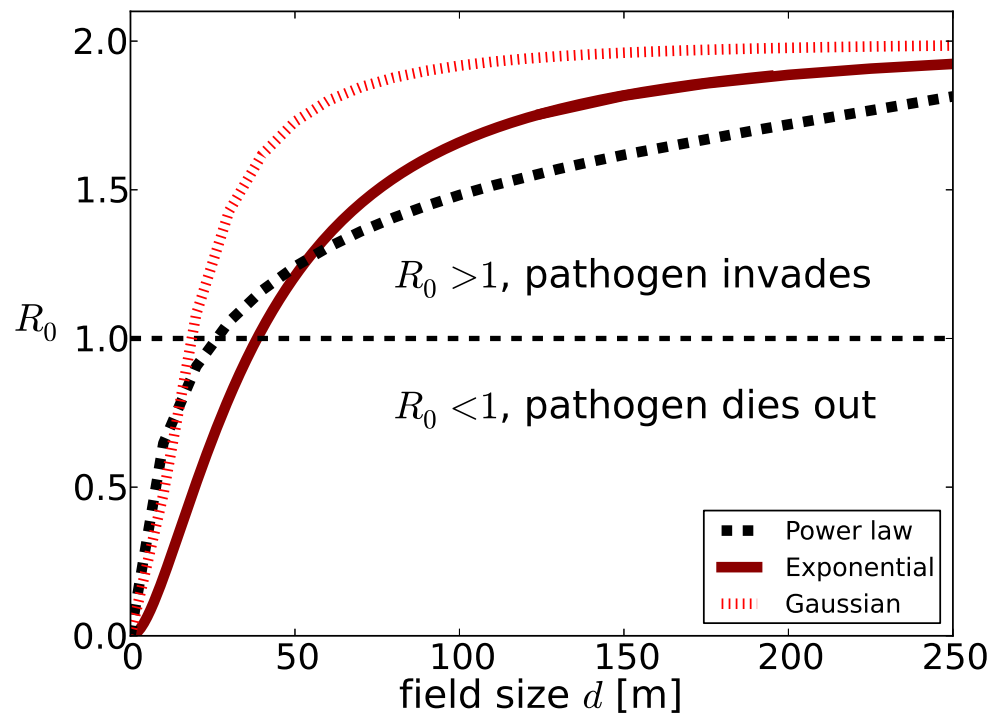


Figure 1

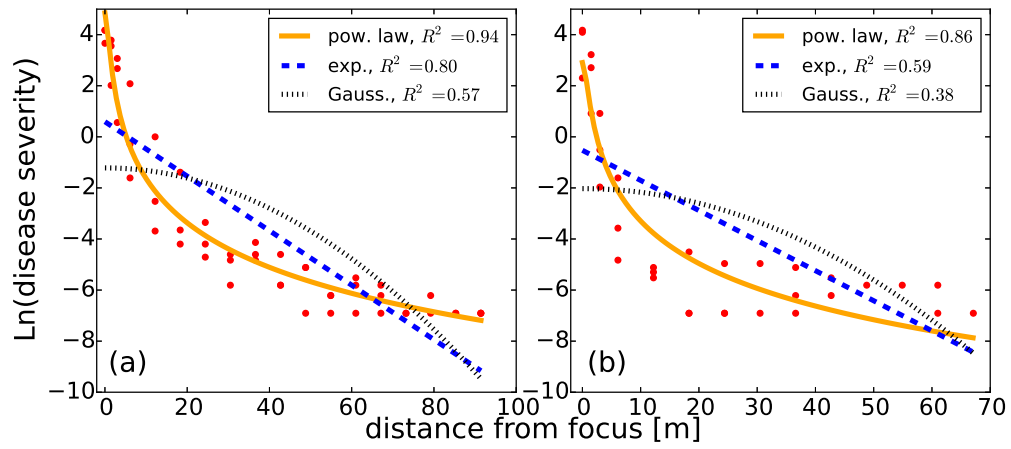


Figure 2

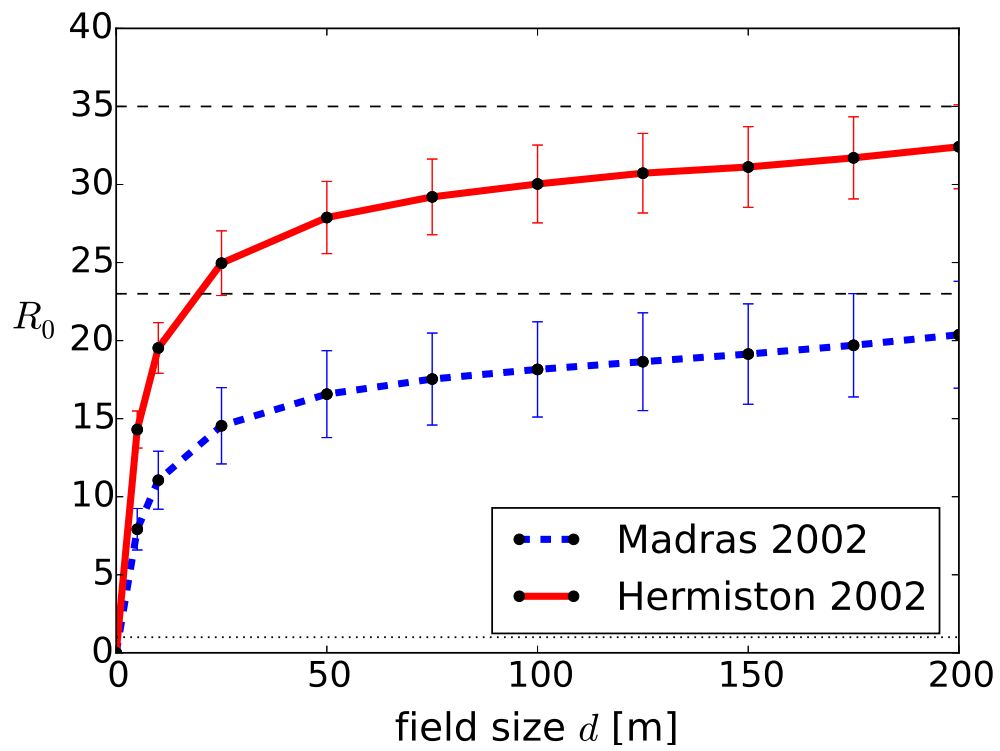


Figure 3

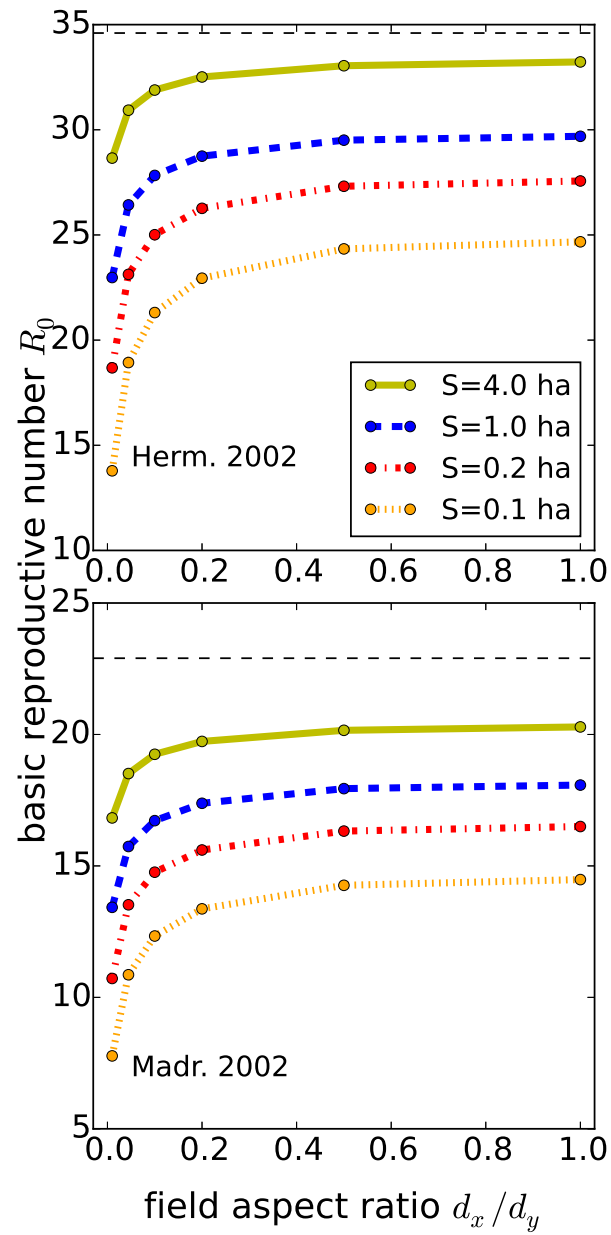


Figure 4

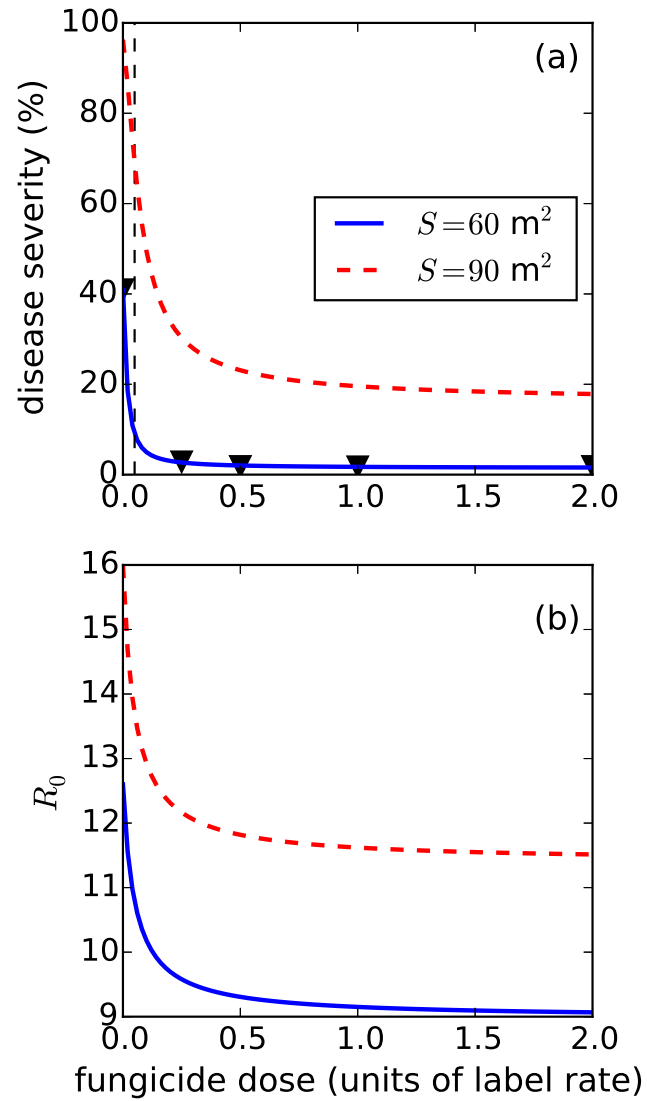


Figure 5